40 kAcm^{-2}, which leads to saturation in the dc to RF conversion efficiency. Therefore, still better performance can be expected from diodes specifically designed for operation on a diamond heat sink.

ACKNOWLEDGMENT

The authors would like to thank Jim Morgan for his skillful machining of the waveguide and other mechanical parts used in this project. They also gratefully acknowledge Pat Stewart's contributions to the machining of the waveguide parts.

REFERENCES

[1] J. Nishizawa and Y. Watanabe, "High frequency Properties of the Avalanching Negative Resistance Diode," Res. Institute Tohoku Univ., Science Rep. 10, 1958, pp. 91–108.

[2] J. Nishizawa, K. Motoya and Y. Okuno, "Submillimeter Wave Oscillation from GaAs TUNNETT Diode," in *Proc 9th Euro. Microwave Conf.*, 1979, pp. 463–467.

[3] M. Pöbl, C. Dalle, J. Freyer and W. Harth, "CW mm-Wave GaAs TUNNETT Diode," *Electron. Lett.*, vol. 26, pp. 1540–1542, 1990.

[4] C. Kidner, H. Eisele and G. I. Haddad, "Tunnel injection transit-time diodes for W-band power generation," *Electron. Lett.*, vol. 28, pp. 511–513, 1992.

[5] H. Eisele, C. Kidner and G. I. Haddad, "A CW GaAs TUNNETT Diode Source for 100 GHz and Above," in *Proc. 22nd European Microwave Conf*, Aug. 24–27, 1992, Helsinki, Finland, pp. 467–472.

[6] H. Eisele, "Selective etching technology for 94 GHz GaAs IMPATT diodes on diamond heat sinks," *Solid-State Electronics*, vol. 32, pp. 253–257 1989.

[7] H. Eisele, "GaAs W-band IMPATT diodes: the first step to higher frequencies," *Microwave J.*, vol. 34, pp. 275–282, 1991.

[8] H. Eisele and G. I. Haddad, "GaAs single-drift flat-profile IMPATT diodes for CW operation in D band," *Electron. Lett.*, vol. 28, pp. 2176–2177, 1992.

[9] H. Eisele, R. Kamoua, G. I. Haddad and C. Kidner, "Active two-terminal devices as local oscillators for low-noise receiver systems at submillimeter wave frequencies," *Archiv für Elektrotechnik*, pp. 15–19, 1994.

[10] B. Fank, J. Crowley, D. Tringali and L. Wandinger, "Basics and recent applications of high-efficiency millimeter wave InP Gunn diodes," in *Proc. 1st Int. Conf. Indium Phosphide Related Materials Advanced Electron. Optical Devices*, Norman, Oklahoma, 1989, SPIE 1144, 1989, pp. 534–546.

[11] I. G. Eddison, et al., "Efficient fundamental frequency oscillation from mm-wave InP n^+-n-n^+ TEOs," *Electron. Lett.*, vol. 17, pp. 758–760 1981.

[12] S. J. J. Teng and R. E. Goldwasser, "High performance second-harmonic operation W-band GaAs Gunn diodes," *IEEE Electron Device Lett.*, EDL-10, pp. 412–414, 1989.

[13] R. Allam and J. Pribetich, "Temperature dependence of electron saturation velocity in GaAs," *Electron. Lett.*, vol. 26, pp. 688–689, 1990.

[14] H. Eisele, "Electron properties in GaAs for the design of mm-wave IMPATTs," *Int. J. Infrared Millimeter Waves*, vol. 4, pp. 345–354, 1991.

[15] H. Eisele, "GaAs W-band IMPATT diodes for very low-noise oscillators," *Electron. Lett.*, vol. 26, pp. 109–110, 1990.

[16] C. C. Chen, R. K. Mains, G. I. Haddad and H. Eisele, "Structure and simulation of GaAs TUNNETT and MITATT devices for frequencies above 100 GHz," in *Proc. 14th Biennial Cornell Conf.*, Ithaca, New York, 1993, pp. 194–202.

[17] J. Freyer, M. Pöbl, W. Harth, L. Gaul and H. Grothe, "70 GHz GaAs TUNNETT diode," in *Proc. 20th European Microwave Conf.*, Budapest, Hungary, 1990, pp. 599–604.

Modelling Drain and Gate Dependence of HEMT 1–50 GHz, Small-Signal S-Parameters, and D.C. Drain Current

Simon J. Mahon and David J. Skellern

***Abstract*— We present refinements to a previously validated HEMT model that improves the model's accuracy as a function of drain bias for simulating d.c. drain current and 1–50 GHz, small-signal S-parameters. By comparing simulation data with experimental data for a 0.4-μm-gate pseudomorphic HEMT, we have been able to establish the accuracy of the refined model, which predicts the device's d.c. current and S-parameters as a function of the applied drain and gate biases to within an accuracy of $\sim$5%. The core of the model and, in particular, its bias dependence, are directly dependent on the HEMT wafer structure and the physical gate length.**

I. INTRODUCTION

In an earlier paper [1], we presented a semi-physical HEMT model based on a 1-D Poisson/Fermi-Dirac solver and a variable boundary electron transport model that produced a good fit to measured S-parameter data as a function of the gate bias for frequencies between 1 and 25 GHz. We later established [2] that the model in [1] was also useful for simulating d.c. drain current and 1–50 GHz S-parameters as a function of the gate bias. However, as will be shown here, this model does not predict the S-parameter (especially S_{22}) drain-bias dependency simultaneously.

In this paper, we present three refinements to the existing model which result in a significant improvement in the model's accuracy as a function of drain bias (especially S_{22}). We demonstrate the capacity of the refined model to simulate the d.c. drain current and the 1–50 GHz, small-signal S-parameters as a function of both the drain bias from near zero to well into the saturated region, and the gate bias from near pinch-off to well into forward bias. S-parameter and d.c. drain-current predictions are compared with experimental data measured on a 0.4 × 250 μm pseudomorphic HEMT similar to that described in [2] at seven drain biases ($V_{\rm ds}$ = 0.1, 0.5, 1.0, 1.5, 2.0, 2.5 and 3.0 V) and nine gate biases ($V_{\rm gs}$ = −1.0, −0.8, −0.6, −0.4, −0.2, 0.0, +0.2, +0.4 and +0.6 V), a total of 63 different biases. The device pinch-off is approximately −1.1 V.

The model represents a HEMT by an equivalent circuit constructed from lumped elements as shown in Fig. 1 in [1]. In the model, we used the composition of the HEMT wafer (including layer thicknesses, compositional fractions and doping density profile), and the gate length and width, as described in Section II and [1], to determine the gate- and drain-bias dependence of the transconductance (g_m), output conductance ($g_{\rm ds}$), gate capacitance ($C_{\rm gs}$) and gate-drain capacitance ($C_{\rm gd}$). S-parameter and d.c. drain current dependence on both gate and drain bias are solely due to the bias dependence of these four elements.

II. MODEL REFINEMENTS

We have made three refinements to the existing model to improve the fit to measured data as a function of drain bias while maintaining a good gate-bias fit. This added three new parameters to the

Manuscript received June 7, 1993: revised April 25,1994.

S. Mahon is with the CSIRO Division of Radiophysics, P.O. Box 76, Epping 2121, Australia.

D. Skellern is with the School of Mathematics, Physics, Computing and Electronics, Macquarie University 2109, Australia.

IEEE Log Number 9406795.

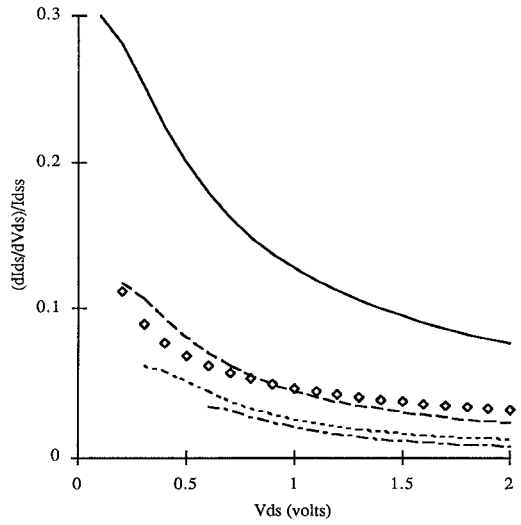

Fig. 1. The numerically calculated value of (4) for $V_{gs} - V_{to} = 0.01$ V(____), 0.2 V (– – – –), 0.5 V (——), and 1.0 V (– - – - –). Also shown is the approximation proposed here (◇), i.e. (6), calculated to best fit the$V_{gs} - V_{to} = 0.2$ V data.

two-dimensional electron gas (2DEG) sub-model and three similar parameters to the parasitic MESFET sub-model. The refinements are as follows:

(1) The electron transport model in [1] is based on the two-region approach of Grebene and Ghandhi [3], and Pucel *et al.* [4]. The gradual channel approximation (GCA) is used in the linear region and constant electron velocity is assumed in the saturated region. For drain voltages less than V_{dss} (i.e. the voltage needed to saturate electron velocity and so create the second region) the GCA determines the drain current. For the 2DEG case

$$I_{ds} = \frac{\mu \cdot q \cdot W}{L_1 + \frac{V_{ds}}{E_1}} \int_0^{V_{ds}} n_s(V_{gs} - V_{cs}) \cdot dV_{cs} \tag{1}$$

where n_s is the 2DEG electron density [1], V_{cs} the channel-source voltage, L_1 the electrical length of the linear region (and hence the gate, since $V_{ds} < V_{dss}$) and E_1 the Rohdin and Roblin constant [5]. In [1] a square-law approximation to (1) was used but we propose a generalized power-law approximation,

$$I_{ds} = \left(1 - \left(1 - \frac{V_{ds}}{V_{dss}}\right)^{\zeta}\right) \cdot I_{dss} \tag{2}$$

where I_{dss} is the current at $V_{ds} = V_{dss}$, and ζ is chosen to give an optimum fit to (1) at a particular gate bias. At $V_{gs} = V_{to} + 0.1$, where the GCA curve is midway between the almost linear $V_{gs} \approx V_{to}$ curve and the sharper curves for $V_{gs} \gg V_{to}$, (2) with $\zeta = 3.20$ agrees with (1) to within 0.52%. By comparison, the square-law approach used in [1], i.e. $\zeta = 2$, differs from (1) by 11% at this gate bias. The refined approach proposed here preserves the physical basis of (1) in a form suitable for circuit simulation. A similar parameter, $m\zeta$, is added to the parasitic MESFET sub-model.

(2) For the 2DEG case, the length of the linear region, once V_{ds} exceeds V_{dss}, is given by [3]:

$$L_1 = L - \frac{2 \cdot d}{\pi} \operatorname{arcsinh}\left(\frac{\pi \cdot (V_{ds} - V_{dss})}{2 \cdot d \cdot E_c}\right), \tag{3}$$

where L is the electrical gate length, E_c the critical field strength and d the distance from the gate to the center of the channel. Substituting (3) into (1), with V_{ds} replaced by V_{dss} in (1), gives the drain current for $V_{ds} > V_{dss}$. However, although the resultant expression for I_{ds} is unsuitable for implementation in circuit simulator tools, we calculate from it the following normalized differential equation (4), shown at the bottom of this page. If we assume I_{dss} to be independent of V_{ds} (see Section III for comment), we can form the same normalized differential from the saturated 2DEG drain current in the earlier model [1]:

$$\frac{dI_{ds}/dV_{ds}}{I_{dss}} = \lambda. \tag{5}$$

In this paper we propose a power-law, channel-length modulation model based on the following approximation to the normalized differential in (4):

$$\frac{dI_{ds}/dV_{ds}}{I_{dss}} = \lambda \cdot \kappa \cdot V_{ds}^{\kappa - 1} \tag{6}$$

generated by choosing λ and κ to give an optimum fit to (4) at $V_{gs} = V_{to} + 0.2$ volts. This is a compromise between the sharp curve at $V_{gs} \approx V_{to}$ and the more linear curves for $V_{gs} \gg V_{to}$. Fig. 1 shows a plot of (4) versus V_{ds} for different V_{gs} (V_{dss} is dependent on V_{gs} [1]), and (6) versus V_{ds} for $V_{gs} = V_{to} + 0.2$ volts. This model gives a much better fit to (4) at a particular V_{gs} than is obtainable with a linear channel-length modulation model such as (5). In general, (6) produces a good fit for most gate biases except near pinch-off. Again the refined approach proposed here preserves the underlying physical basis of (4) in a form suitable for circuit simulation. So, for $V_{ds} > V_{dss}$, we write $I_{ds} = I_{dss} \cdot (1 + \lambda \cdot V_{ds}^{\kappa})$ in the refined model, instead of $I_{ds} = I_{dss} \cdot (1 + \lambda \cdot V_{ds})$ as in [1]. A similar parameter, $m\kappa$, is added to the parasitic MESFET sub-model.

(3) The shift in FET threshold voltage as a function of V_{ds} (i.e. drain feedback effect) can be predicted by a 2-D numerical or quasi-2-D analytical Poisson solver such as Liu *et al.* [6], but not by a 1-D Poisson solver such as in [1]. This effect was modelled in [1] as a linear function of V_{ds} which is a useful approximation for long gate lengths. However, Liu *et al.* [6] showed that a linear term plus a term proportional to $\sqrt{V_{ds}}$ is more appropriate for short gate FETs. Rather than follow Liu exactly, we have maintained the style of the first two refinements and introduced a nonlinear dependence on V_{ds} for the drain feedback effect by replacing (for the 2DEG case) $V_{gs'} = V_{gs} + \eta \cdot V_{ds}$ in [1] by $V_{gs'} = V_{gs} + \eta \cdot V_{ds}^{\varphi}$ in the refined model. A similar parameter, $m\varphi$ is added to the parasitic MESFET sub-model. The values of φ and $m\varphi$ are chosen by the optimizer (Section III).

III. Results and Discussion

The fit to measured data was obtained by defining error metrics between the measured and modelled data. The absolute drain-current error, $E_{I_{ds}}$, is defined as the rms difference between the measured

$$\frac{dI_{ds}/dV_{ds}}{I_{dss}} = \frac{L + \frac{V_{dss}}{E_1}}{E_c \cdot \left(L + \frac{V_{dss}}{E_1} - \frac{2\,d}{\pi} \cdot \operatorname{arcsinh}\left(\frac{\pi\,(V_{ds} - V_{dss})}{2\,d\,E_c}\right)\right)^2 \cdot \sqrt{\left(\frac{\pi\,(V_{ds} - V_{dss})}{2 \cdot d\,E_c}\right)^2 + 1}} \tag{4}$$

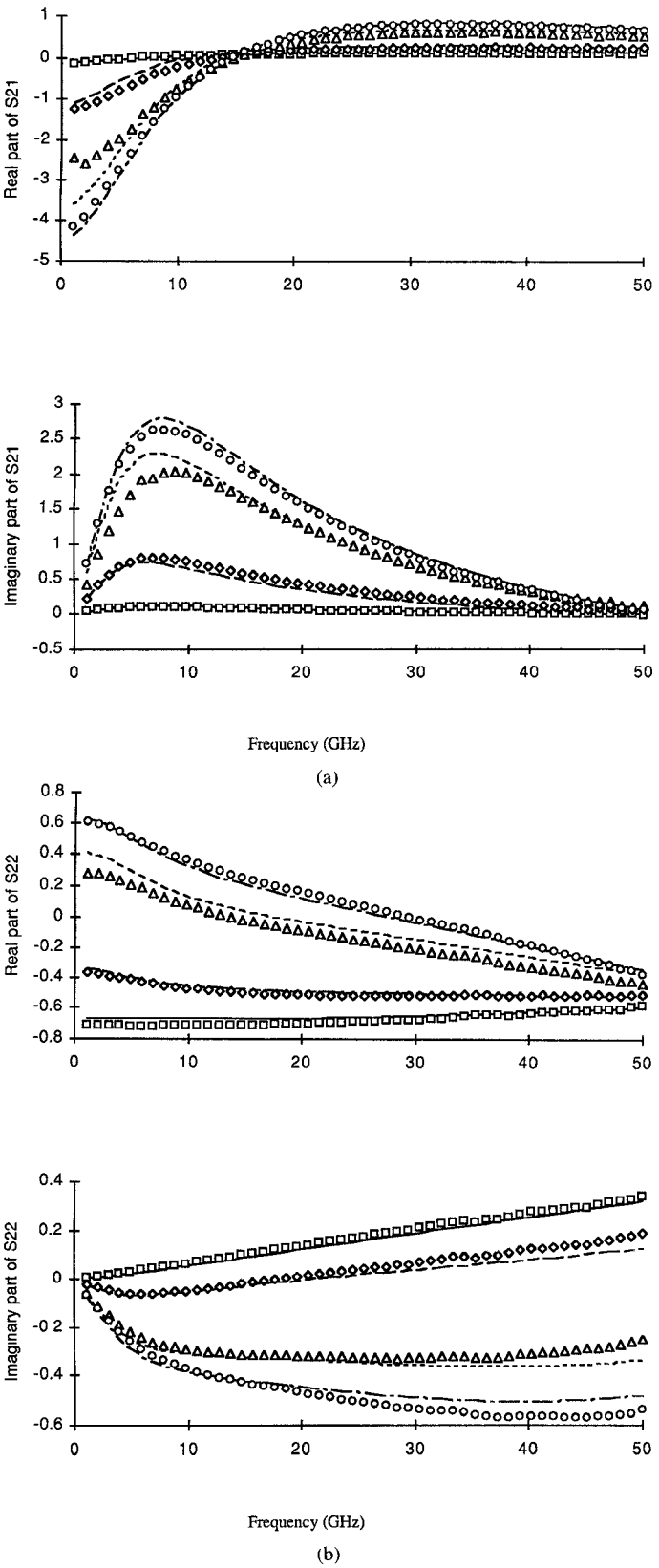

Fig. 2. The real and imaginary parts of the measured (symbols) and simulated (lines) S-parameters for Case (C) as a function of V_{ds} and frequency at $V_{gs} = -0.4$ V: (a) S_{21} and (b) S_{22}. $V_{ds} = 0.1$ V (□ and ——), 0.5 V (◇ and – – – –), 1.0 V (△ and - - - -), and 3.0 V (o and – - – - –).

and simulated currents with summation taken over all bias points. The absolute S-parameter errors, $E_{S_{ij}}(i,j = 1,2)$, are defined as the rms difference between the measured and simulated currents with

TABLE I

ABSOLUTE AND NORMALIZED ERRORS DESCRIBING THE FIT TO EXPERIMENTAL D.C. DRAIN CURRENT AND 1–50 GHz S-PARAMETERS OVER THE 63 BIASES FOR CASE A. MODEL IN [1] WITH λ AND $m\lambda$ CHOSEN BY THE OPTIMIZER, ζ AND $m\zeta$ SET TO 2, AND κ, $m\kappa$, φ AND $m\varphi$ SET TO 1. CASE B: REFINED MODEL WITH $\zeta, m\zeta, \lambda, m\lambda$ κ AND $m\kappa$ CALCULATED USING SECTION II AND φ AND $m\varphi$ CHOSEN BY THE OPTIMIZER CASE C: REFINED MODEL WITH $\zeta, m\zeta, \lambda, m\lambda, \kappa$ AND $m\kappa$, φ AND $m\varphi$ CHOSEN BY THE OPTIMIZER

Parameter	Case A error		Case B error		Case C error	
	Absolute	Norm (%)	Absolute	Norm (%)	Absolute	Norm (%)
Ids	3.39 mA	3 39	4.63 mA	4.64	2.28 mA	2.29
S_{11}	0 0530	5 33	0 0512	5.15	0.0513	5.16
S_{12}	0 0162	6 31	0.0172	6.70	0.0159	6.20
S_{21}	0.242	5.22	0.166	3.57	0.179	3.87
S_{22}	0.0957	11.88	0.0590	7.32	0.0568	7.04
Average	–	6.43	–	5.48	–	4.92

summation taken over all frequencies and all bias points. Three cases are examined in this section:

(A) the model in [1], i.e. ζ and $m\zeta$ set to 2, $\kappa, m\kappa, \varphi$ and $m\varphi$ set to 1, and λ and $m\lambda$ optimized;

(B) the refined model with $\zeta, m\zeta, \lambda, m\lambda, \kappa$ and $m\kappa$ is calculated from the theory in Section II at the noted V_{gs} values and φ and $m\varphi$ optimized;

(C) the refined model with $\zeta, m\zeta, \lambda, m\lambda, \kappa, m\kappa, \varphi$ and $m\varphi$ chosen by an optimizer.

The remaining model parameters are either calculated from the wafer structure and gate length using the theory in [1] or chosen by a complex-search optimizer to minimize the unweighted average of the normalized I_{ds} and S-parameter errors. Normalizing the absolute rms errors by the maximum parameter magnitude prevents the numerically smaller parameters, such as S_{12} and I_{ds}, being swamped by the numerically larger parameters, such as S_{21}.

The error metrics quantifying the model fit to experimental data for (A), (B) and (C) are shown in Table I. The results show that the earlier model is unable to simulate S_{22} accurately and that the refinements proposed here, i.e. (B) and (C), enable a significant improvement in the simulation accuracy for S_{22} and a modest improvement in S_{21} accuracy. The values calculated for (B), using the theory and V_{gs} values from Section II, are $\zeta = 3.20$, $m\zeta = 1.66$, $\lambda = 0.103$, $m\lambda = 0.572$, $\kappa = 0.457$ and $m\kappa = 0.123$. As noted in Section II, these values were calculated at a V_{gs} chosen as representative by inspecting the solutions to (1) and (4), i.e. Fig. 1 for the latter equation. For (C) the values of are chosen by the optimizer to be $\zeta = 2.36$, $m\zeta = 1.90$, $\lambda = 0.0003$, $m\lambda = 0.0004$, $\kappa = 0.70$ and $m\kappa = 0.49$. In allocating values for $\zeta, m\zeta, \lambda, m\lambda, \kappa$ and $m\kappa$ the optimizer in (C) is, in effect, choosing the most appropriate value of V_{gs} at which to solve (1) and (4) for the particular set of measured data. Hence, the values in (C) differ from those calculated for (B). The dependence of I_{dss} on V_{ds} resulting from the drain feedback effect and the resultant inaccuracy induced in (5) and (6) also results in differing values of $\lambda, m\lambda, \kappa$ and $m\kappa$. In a more complete model $\zeta, m\zeta, \lambda, m\lambda, \kappa$ and $m\kappa$ may contain a V_{gs} dependency although this would increase model complexity.

Fig. 2 illustrates the agreement between the measured and simulated S_{21} and S_{22} for this device as a function of frequency and drain bias with $V_{gs} = -0.4$ volts. The simulated data are from (C) as it produced better agreement than (B). The S_{11} data are insensitive to changes in drain bias and hence are not shown. The S_{12} data are sensitive to drain bias, especially above about 10 GHz, but have been omitted for brevity. The S_{21} and S_{22} data are sensitive to

drain bias and this is well matched by the model in general, although the agreement is poorer for the 1.0 V drain bias. Graphs comparing measured and simulated S-parameters as a function of gate bias show good agreement. The fit to the $I_{\rm ds}$ data is good in general except near pinch-off where the independence of λ, $m\lambda$, κ and $m\kappa$ from $V_{\rm gs}$ may be a source of some model inaccuracy.

ACKNOWLEDGMENT

We thank John Archer for useful discussions and Tina Fiocco for measuring the S-parameter and drain current data. Both are from the CSIRO Division of Radiophysics.

REFERENCES

[1] S. J. Mahon, D. J. Skellern and F. Green, "A technique for modelling S-parameters for HEMT structures as a function of gate bias," *IEEE Trans. Microwave Theory Tech.*, vol. MTT-40, pp. 1430–1440, July 1992.

[2] S. J. Mahon, M. Chivers, and D. J. Skellern, "Simulation of HEMT DC drain current and 1 to 50 GHz S-parameters as a function of gate bias," *IEEE Trans. Microwave Theory Tech.*, vol. MTT-41, pp. 1065–1067, June/July 1993.

[3] A. B. Grebene and S. K. Ghandhi, "General theory for pinched operation of the junction-gate FET," *Solid-State Electron.* New York: Pergamon, 1969, vol. 12, pp. 573–589.

[4] R. A. Pucel, H. A. Haus, and H. Statz, "Signal and noise properties of gallium arsenide microwave field-effect transistors," *Adv. Electronics Electron. Phys.*., vol. 38, pp. 195–265, 1975.

[5] H. Rohdin and P. Roblin, "A MODFET dc model with improved pinchoff and saturation characteristics," *IEEE Trans. Electron Devices*, vol. ED-33, no. 5, pp. 664–672, May 1986.

[6] Z.-H. Liu, C. Hu, J.-H. Huang, T.-Y. Chan, M.-C. Jeng, P. K. Ko, and Y. C. Cheng, "Threshold voltage model for deep-submicrometer MOSFETs," *IEEE Trans. Electron Devices*, vol. ED-40, no. 1, pp. 86–95, Jan. 1993.

Nonlinear Mixer Gain Calculations for Josephson Junctions

Hoton How, Ta-Ming Fang, Carmine Vittoria, and Allen Widom

***Abstract*—We have numerically solved the steady-state solutions of the initial value problem associated with a current-driven Josephson weak-link junction shunted by an Ohmic resistance. The nonlinear mixing action of the junction leads to Shapiro steps in the dc response with step height in units of the mixing frequency. Mixer gains have been calculated with a wide range of parameter values and intrinsic chaos are observed whenever Shapiro steps are prevalent.**

I. INTRODUCTION

The current-driven Josephson weak-link can be formulated in terms of the resistively shunted junction (RSJ) model that may be cast in the form of a first-order differential equation, shown in (1). In integrating the equation from $t = 0$ to obtain a steady-state solution, one is faced with the problem that the initial phase, $\phi(0)$, across the junction is unknown. The solution to (1) is very sensitive to the initial condition on ϕ, and a slight change in the initial condition may result in chaotic behavior of ϕ [1]. In the absence of noise the steady-state solution, if it exists, the system is required to return to its initial phase of 2π after one period of the sinusoidal drive (or drives). This determines the asymptotic solution of the system and results in Shapiro steps in units of the mixing frequency in the dc response. We found that intrinsic chaos is most likely to be observed near these step edges. In the presence of noise, the system may not be able to return to its initial phase after one period, and hence no steady-state solution is possible. This leads to extrinsic chaos, since it can be induced by external noise [2]. Traditionally, the Josephson mixer gain is calculated from a linearized perturbation theory [3]–[7]. In the linearized solution, one assumes that the response in ϕ can be approximated by a linear combination of the dc and rf responses, since the rf excitation amplitude is small compared to the dc biasing current. As such, one can then apply circuit theory analysis as in the so-called "conversion matrix method.&r Here we present a systematic method by which the gain is calculated in the nonlinear regime. We find that the mixer gain can be much greater than unity for small carrier current and large local oscillator current under optimal coupling of the load resistance to the junction-shunting circuit. This high gain effect of a Josephson mixer has also been observed experimentally [8].

Manuscript received September 14, 1993; revised April 7, 1994. This work was supported by the National Science Foundation.

H. How and T.-M. Fang are with the Massachusetts Technological Laboratory, Inc., Belmont, MA 02178 USA.

C. Vittoria and A. Widom are with Northeastern University, Boston, MA 02115 USA.

IEEE Log Number 9406808.

II. CALCULATION

The Josephson mixer circuit shown in the inset of Fig. 3 leads to the following first-order equation [6]:

$$i_D + i_S \cos\omega_S t + i_L \cos\omega_L t + i_N(t) - \sin\phi = \tau(d\phi/dt), \quad (1)$$

where ϕ is the phase difference of the superconducting wave function across the junction and i_D, i_S, i_L, and i_N are, respectively, the dc current, rf currents at the signal carrier frequency, ω_S, the local-oscillator frequency, ω_L, and the noise current, all normalized to the critical current of the junction, I_c. In (1), $\tau = \hbar/2eR_GI_c$, $R_G^{-1} = Z_G^{-1} + R^{-1}$ and R and Z_G are the shunting and external load resistances. We assume the thermal current i_N possesses normal distribution with $\langle i_N\rangle = 0$ and $\langle i_N^2\rangle = 4k_BTB/RI_c^2$, where B denotes the frequency bandwidth of the detector and T is the junction temperature. Note that in (1) we have ignored the shunting capacitance across a Josephson weak-link junction, since it is assumed to be small. Therefore, if the initial value of ϕ is known at $t = 0$, denoted as α, $\phi(\alpha; t)$, can be calculated by integrating (1) utilizing a fourth-order Runge-Kutta algorithm in double-precision arithmetic.

If there are no rf currents and only a dc current applied to the junction, the solution is straightforward, since the differential flux across the junction is zero, and hence $\alpha = \sin^{-1}(i_D/I_c)$. In a typical mixer experiment, two rf currents and one dc current source are applied to the junction simultaneously. If the dc source is applied firstly, ϕ is unknown upon application of the rf currents. The onset times of these sources may not be precisely noticed under most experimental conditions. Similarly, if we reverse the experiment, ϕ is still an unknown quantity in the presence of all three sources. The dilemma is then what to choose for an initial condition on ϕ in order to uniquely solve for ϕ as a function of time. In this paper, we are interested in the steady-state solution after all the transients have died out. One can solve this problem empirically by choosing different α values and noting what is the response of ϕ after one common period T, $\phi(\alpha; T)$. Here, we assume T to be the period at the mixing frequency, which should not be confused with the symbol used for temperature. If one plots the phase change, $\phi(\alpha; T)$-α, as a function of α, one may find a value of α, say α_o, at which the phase change is